SPECTROSCOPIC ANALYSIS OF THE INTERACTION BETWEEN SILVER NANOPARTICLES AND TRYPSIN**

Min Liu, Yi Li, Luo Li, Xiuyun Sun, Jiansheng Li, Rui Lu*

Jiangsu Key Laboratory of Chemical Pollution Control and Resources Reuse,
School of Environmental and Biological Engineering at Nanjing University of Science and Technology,
Nanjing 210094, China; e-mail: rlu@njust.edu.cn

The rapid development of nanoparticles (NPs) and their broad applications in medicine caused concerns about biological effects and biosafety. Here, the interaction of silver NPs (AgNPs) and trypsin is studied with ultraviolet-visible spectra, circular dichroism, and fluorescence spectra. Trypsin is exposed to various sizes and concentrations of AgNPs. The intensities of the trypsin ultraviolet-visible absorption peaks are proportional to the AgNP concentration and size. In the circular dichroism spectra, there was evidence that AgNPs affected the secondary structure of trypsin. Fluorescence spectra show that the formation of the protein-nanoparticle complexes alters the protein chromophore chemical environment or structure and quenches its fluorescence. Hence, the extent of AgNP binding of trypsin depends on both NP concentration and size, and changes the AgNPs physicochemical properties as well as the trypsin secondary structure. With regard to nanomaterial safety, the interaction of NPs with proteins must be explored further for establishing NP toxicity and design guidance.

Keywords: *Ag nanoparticles, trypsin, interaction mechanism, ultraviolet-visible, circular dichroism, fluorescence spectra.*

СПЕКТРОСКОПИЧЕСКОЕ ИССЛЕДОВАНИЕ МЕХАНИЗМА ВЗАИМОДЕЙСТВИЯ НАНОЧАСТИЦ СЕРЕБРА С ТРИПСИНОМ

M. Liu, Y. Li, L. Li, X. Sun, J. Li, R. Lu *

УДК 535.372;543.42:620.3

Школа экологической и биологической инженерии
Нанкинского университета науки и технологий, Нанкин 210094, Китай; e-mail: rlu@njust.edu.cn

(Поступила 26 ноября 2019)

Исследовано взаимодействие НЧ серебра (НЧ Ag) с трипсином с применением спектров УФ-видимого диапазона, флуоресценции и кругового дихроизма. Трипсин подвергается воздействию НЧ Ag различных размеров и концентраций. Интенсивность пиков поглощения трипсина в спектре УФ-видимой области пропорциональна концентрации и размеру НЧ Ag. Спектры кругового дихроизма свидетельствуют о влиянии НЧ Ag на вторичную структуру трипсина. Спектры флуоресценции показывают, что образование комплексов белок–наночастица изменяет химическое окружение или структуру белкового хромофора и тушит его флуоресценцию. Следовательно, степень связывания НЧ Ag с трипсином зависит как от концентрации, так и от размера НЧ и изменяет физико-химические свойства НЧ Ag, а также вторичную структуру трипсина. Относительно безопасности наноматериалов, для установления токсичности НЧ и руководства по их проектированию необходимо дополнительно изучать взаимодействие НЧ с белками.

Ключевые слова: *наночастицы серебра, трипсин, механизм взаимодействия, УФ-видимый диапазон спектра, круговой дихроизм, спектр флуоресценции.*

** Full text is published in JAS V. 88, No. 1 (http://springer.com/journal/10812) and in electronic version of ZhPS V. 88, No. 1 (http://www.elibrary.ru/title_about.asp?id=7318; sales@elibrary.ru).

Introduction. Nanoparticles (NPs) have sizes over the range 1–100 nm [1]. Interactions of atoms and the fluctuation of electrons in nanoscale materials change with respect to bulk properties, resulting in specific NP effects due to surfaces, volume, quantum size [2], macroscopic quantum tunneling [3], and dielectric confinement. Usually, NPs have large adsorption capacities, high surface-area-to-volume ratios, ability to bind molecules, and strong physical properties on account of their quantum effect, small size effect, and large specific surface area. These features enable silver NPs (Ag NPs) to easily interact with pathogenic microorganisms and have a wide range of antibacterial properties and long sterilization activities [4].

When NPs enter a biological system, they could encounter biological macromolecules such as proteins. They could inhibit protein self-aggregation, then replace the original core, and cause surrounding proteins to self-aggregate with the NP as a core [5]. After protein binding on the NPs surface, a "protein corona" structure will form, which usually changes the physicochemical properties of both the NP and the protein [6]. The NP surface chemistry, surface charge, and hydrophilicity can all change after protein absorption. For proteins, the most important effects after binding to NPs are conformational changes, which can be either reversible or irreversible, depending on the NP type, size, concentration and surface chemistry. Protein binding to NPs can be the result of van der Waals, electrostatic or hydrophobic interactions, as well as hydrogen bonding and π-π stacking [7, 8]. Van der Waals forces are generally considered to be the primary protein-NP interactions [9].

Trypsin is an indispensable proteolytic enzyme in most vertebrates. It has a molecular mass of 23,000 and consists of 223 amino acid residues, with four tryptophan residues and six pairs of disulfide bonds [10]. In humans, trypsin is one of the most important digestive proteases excreted by the pancreas into the small intestine. It is also widely expressed in other tissues of the human body, such as the esophagus, stomach, liver, lungs, intravascular epithelial cells, spleen leukocytes and skin cells [11]. Thus, trypsin plays a vital role in the human body and has received considerable attention. For example, Gombos has shown that the enzyme has been widely used in physiological processes, apoptosis, signal transduction, hemostasis, immune responses, and the food industry [12]. Therefore, it is particularly essential to understand the effects of NPs on trypsin, and to study the interaction mechanism with different impact factors. Furthermore, understanding the interaction between NPs and proteins can encourage awareness of the unique NP physical and chemical properties and to use NPs safely and effectively.

Here, four different sizes (4, 20, 30, and 45 nm) of uniform and dispersed Ag NPs were prepared via seed growth. Their sizes, morphologies, and homogeneities were characterized with transmission electron microscopy (TEM), ultraviolet-visible (UV-Vis) spectroscopy, and dynamic light scattering (DLS). Silver NP size effects on trypsin were investigated with multiple spectroscopic methods. Circular dichroism (CD) spectroscopy was used to characterize secondary structure changes, while UV-Vis and fluorescence spectroscopy were used to study binding affinities and ratios of trypsin to Ag NPs. This in-depth analysis will be helpful for the understanding of biological effects and potential physiological and toxicological effects of Ag NPs. It will also provide a scientific basis for the interaction of Ag NPs with other proteins and biological molecules.

Experimental. Silver nitrate ($AgNO_3$) was purchased from Sinopharm Chemical Reagent Co., Ltd. (Beijing, China). Trisodium citrate dihydrate ($C_6H_5Na_3O_7 \cdot 2H_2O$) was obtained from Shandong West Asia Chemical Industry Co., Ltd. (Shandong, China). Trypsin was purchased from Shanghai Yishi Chemicals Co. Ltd. (Shanghai, China). Deionized water with a resistance of 18 MΩ ·cm was used in all the experiments.

Sodium phosphate sodium buffer solution (PBS) with pH 7.4 was prepared. A trypsin solution was prepared and diluted to different concentrations in 0.1 mmol/L PBS (pH 7.4). All solutions were stored at 4°C.

Silver NPs were prepared as reported previously [13]. To a round-bottom flask, 20 mL of 1% (w/v) citrate solution and 75 mL of water were added, and the whole heated to boiling for 15 min. Then 1.7 mL of a 1% (w/v) $AgNO_3$ solution and 2 mL of a 0.1% (w/v) freshly prepared $NaBH_4$ solution were added to the mixture in turn. The reaction solution was boiled while stirring for 1 h and then cooled to room temperature. The resulting Ag NPs were used as starter seeds. Two milliliters of 1% citrate solution was mixed with 80 mL of water and boiled for 15 min with a heating mantle. Next, 10.0 mL of the starter seed solution and 1.7 mL of a 1% $AgNO_3$ solution were added with vigorous mechanical stirring. The stirring continued for 1 h while refluxing, and the solution was then cooled to room temperature to yield 20-nm Ag NPs. To obtain 30-nm Ag NPs, the above steps were repeated. The, 2 mL of 1% citrate solution was added to the reaction solution together with 1.7 mL of 1% $AgNO_3$ solution. The refluxing continued for another hour with vigorous stirring. The same operation was repeated again, and the reaction solution was cooled to room temperature. To obtain 45-nm Ag NPs, the 30-nm Ag NPs were used as seeds. Then 2 mL of 1% citrate solution was

mixed with 80 mL of water, and the whole boiled for 15 min. Next, 10.0 mL of the seed solution was added while stirring, followed by the addition of 1.7 mL of 1% $AgNO_3$ solution. The reaction solution was boiled with vigorous mechanical stirring for 2 h and then cooled to room temperature. The Ag NPs were dissolved in deionized water and diluted to different concentrations.

The Ag NP suspensions were completely ultrasonicated. Then, Ag NPs-trypsin complex in PBS was mixed with 2% sodium phosphotungstate solution at a volume ratio of 1:1, and 60 μL of the suspension was placed on a TEM copper grid and dried in air. Imaging of the samples was performed with a 120-kV acceleration voltage on a JEOL 1230 TEM (JEOL Ltd., Japan).

The Ag NPs solutions of (0.5, 1.0, 2.0, 3.0, 4.0, and 5.0 mmol/L) and trypsin at 2.5×10^{-4} mol/L were incubated in PBS buffer at 4°C for 3 h. Then UV-Vis spectra of the mixed solutions were acquired over the range of 250–500 nm with a PerkinElmer Lambda 25 equipped with a 1.0-cm quartz cuvette.

Samples were prepared by mixing a 1.0×10^{-5} mol/L solution of trypsin with different concentrations of Ag NPs. After storage in 4°C for 3 h, fluorescence spectra were acquired with a fluorescence spectrophotometer (HITACHI F-7000) equipped with a 1.0-cm quartz cuvette. The emission wavelengths ranged over 295–450 nm with 280-nm excitation. The widths of both the excitation and emission silts were 5.0 nm.

CD spectra of trypsin in the absence and presence of Ag NPs were obtained with a J-810 Spectrometer (Jasco, Tokyo, Japan) over the range of 200–250 nm. The Ag NP solution was added to the trypsin solution (10^{-5} mol/L) in a 1:1 volume ratio and reacted for 3 h at 4°C. The CD spectra were acquired in a quartz cell with a 0.1-cm optical path. The scanning speed was 100 nm/min, and each sample was scanned six times to increase the signal-to-noise ratio. To analyze the spectrum, the second derivative peak was determined with Peak Fit software (Sea Solve Software, USA).

Trypsin (200 μg/mL) in PBS (0.1 mmol/L pH 7.4) was mixed with different concentrations of Ag NPs (0, 0.5, 1.0, 2.0, 3.0, 4.0, and 5.0 mmol/L) at 37°C for 30 min [14]; 5 mL of 1% (w/v) casein substrate suspension was added to the mixture. After 10 min, the reaction was stopped with 1.0 mL of 30% trichloroacetic acid solution, and the precipitates were centrifuged at 12,000 rpm for 10 min. The supernatant was extracted for later use, and the UV-Vis absorption at 275 nm was measured. The trypsin activities in the absence and presence of different concentrations Ag NPs were then analyzed.

Results and discussion. Ag NPs were characterized with TEM, UV-Vis spectroscopy, and DLS. The TEM and DLS images indicate that the Ag NPs have consistent sizes and uniform distributions. TEM images reveal the homogeneous spherical shapes for each size range (4, 20, 30, and 45 nm, respectively). In Figure S1, UV-Vis spectra have maximum absorption peaks at 390, 392, 403, and 414 nm, for the 4, 20, 30, and 45-nm Ag NPs, respectively. The symmetric narrow peaks confirmed uniform sizes, good monodispersity, and spherical shapes. DLS is a light scattering technique that is widely used to determine hydrodynamic diameters of nanoparticles. However, it is difficult to distinguish scattered light produced from proteins and NPs having similar sizes. Therefore, only when the Ag NPs are much larger than proteins (10 nm) can they be distinguished. The formation of protein crowns determines the magnitude and variation of the hydrodynamic radius of the nanoparticle-protein complex [15]. As illustrated in Fig. S2, we performed DLS for four different Ag NP size and plotted the relevant histograms. Because of the good agreement in all the above characterizations, it can be confirmed that the Ag NPs target sizes were successfully synthesized.

CD is a widely recognized tool for studying secondary structure of proteins [16]. Bio-macromolecules such as proteins have several chromophores that can cause CD spectral changes. When the plane of circularly polarized light passes through an optically active protein, the difference in absorbance of left- and right-components changes their relative amplitudes and converts the circularly polarized light vector into an elliptical polarization. This is the circular dichroism of the protein. For example, Gautam et al. found that the CD spectra of bovine serum albumin conjugated with Ag NPs showed considerable changes in its secondary structure [17]. Gebregeorgis et al. also found changes in its secondary structure because of an association with silver ions or reduced silver [18].

Proteins are composed of amino acids linked by peptide bonds, where the alpha-carboxyl group of one amino acid is linked to the alpha-amino group of another amino acid to form an acid-amine bond. In proteins or polypeptides, the primary optically active groups are peptide bonds composed of aromatic amino acid residue and disulfide bridges in the peptide chain backbone. The amide chromophore of the peptide bond dominates the far-UV CD spectrum over the range 190–250 nm [19], which contains the secondary structural conformational information of the protein. The α-helix conformation usually exhibits a negative band around 208 nm, near 222 nm because of its strong hydrogen-bonding environment, and has a positive band near 192 nm. The β-sheet conformation shows a negative band at 216 nm, strong positive bands at 195 and

198 nm, and a negative band at around 175 nm [20, 21]. However, the positions and amplitudes of these bands are variable, and the resulting prediction of the β-sheet structure is not as good as that for the α-helix. Therefore, when using CD to study protein secondary structures quantitatively, an α-helix based protein is mostly used for detection [22].

We examined CD spectra over the range 200–250 nm to monitor secondary structure changes of trypsin in the absence and presence of Ag NPs. Because of the strong hydrogen bonding in the α-helix, the far-UV CD spectra have two negative minima near 208 nm caused by the π-π* transition of the trypsin α-helix [23]. The intensities of the two minima indicate the degree of helicity in the protein.

The reduction in their intensities reflects changes in the secondary structure of the protein. In Fig. 1, the CD spectra show a decrease near 208 nm for the trypsin-Ag NPs complex relative to that for pure trypsin, which indicates an increment of the α-helix structure and a blue shift from the unfolding structure of trypsin. A quantitative analysis of the changes in the secondary structure of trypsin when interacting with Ag NPs is summarized in Table 1. The α-helix in natural trypsin is 8.1%, the β-sheet is 34.5%, the β-turn is 10.3%, and the random coil is 47.1%. When Ag NPs were mixed into the protein solution, the α-helix increased slightly to 9.3%, β-sheet decreased to 29%, the β-turn increased to 17.2%, and the random coil decreased slightly to 44.5%. These results reflect the secondary structure changes of trypsin in the presence of Ag NPs.

When UV-Vis spectroscopy is used to study the optical properties of NPs, the intensity and position of the plasma oscillation peak is related to the size, shape, and dispersion. As shown in Fig. 2, the UV-Vis absorption spectra of the trypsin-Ag NPs complex has a maximum at 278 nm due to the π-π* electronic transitions of aromatic amino acid residues [24]. The absorption intensity at 278 nm increased with the concentration of Ag NPs, which indicates an interaction of the trypsin peptide chain portion with the Ag NPs. Additionally, Ag NPs with diameters over the range 4–45 nm exhibited a characteristic surface plasma band centered at 390–414 nm. After adding trypsin to Ag NPs solutions, the Ag NP absorption bands of various sizes exhibited shifts from 390 to 414 nm, as well as significant increases in the intensity of the plasma band. Normalized trypsin absorbance changes in the presence and absence of Ag NPs are shown in Figs. S3–S6, where the absorption maxima of the complexes shifted after trypsin interacted with different sizes of Ag NPs. The possible reason for the shift is the interaction between the NPs and protein [25] and the increased Ag NP sizes with trypsin adsorption.

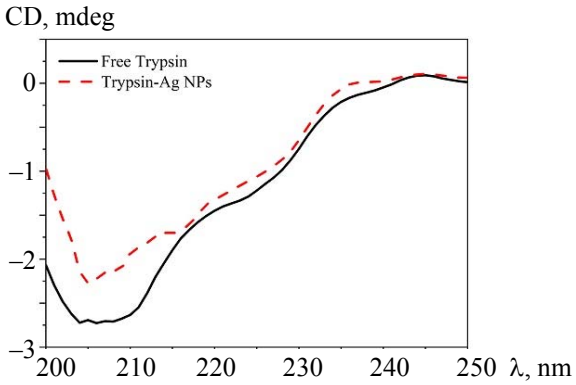

Fig. 1. Circular dichroism spectra after smoothing of trypsin in the absence and presence of Ag NPs.

TABLE 1. Changes in Trypsin Secondary Structure Composition Induced by Complex with Ag NPs

System	α-helix	β-sheet	β-turn	Random coil
Free Trypsin	8.1	34.5	10.3	47.1
Trypsin-Ag NPs	9.3	29.0	17.2	44.5

The shifts and increased plasmon resonances also indicated Ag NPs aggregations of mediated by the trypsin [26]. This indicates that the trypsin adsorbed on the Ag NP surface forms a protein corona, and that this interaction could also affect the particle size distributions and the surface plasma band of the NPs.

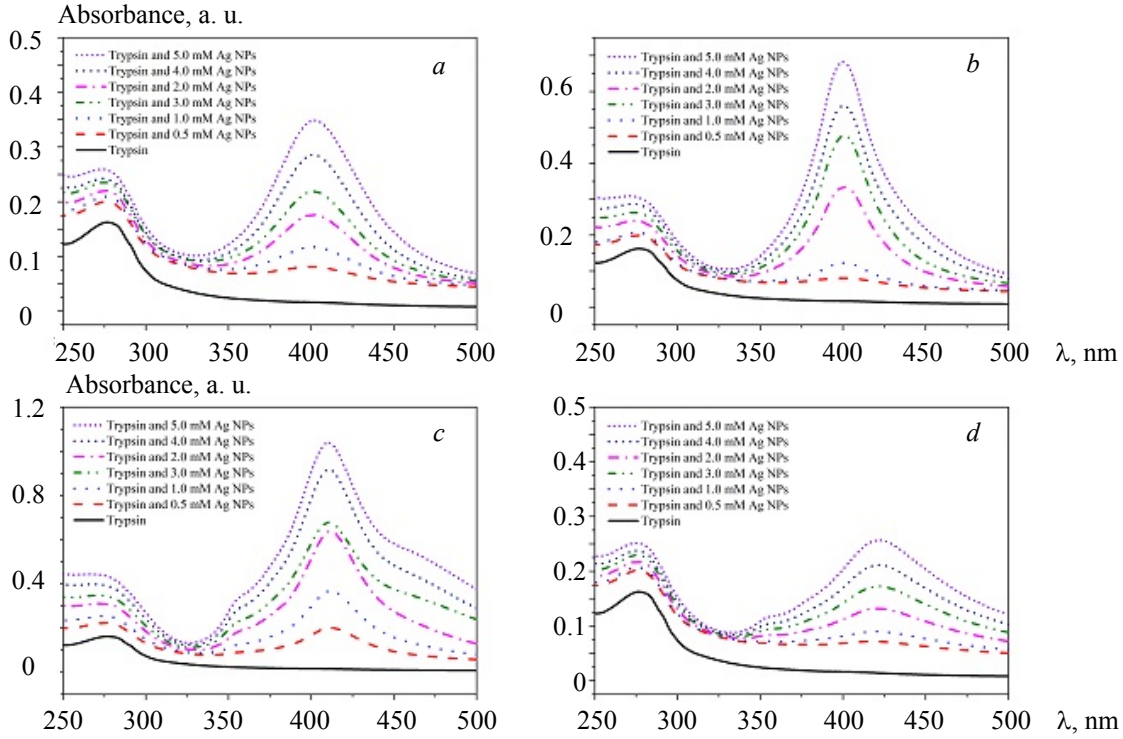

Fig. 2. UV-Vis spectra of trypsin in the absence and presence of Ag NPs of different sizes: 4 (a), 20 (b), 30 (c), and 45 nm (d). The concentration of trypsin is 1.0×10^{-5} mol/L, and the concentration of Ag NPs is in the range of 0–5 mmol/L.

Fluorescence analysis has the advantages of high selectivity, high sensitivity, and low sample consumption. Valuable information about the change in polarity around the fluorophore can be obtained [27]. Many significant biological reactions occur in a few seconds [28], such as changes in protein conformation, rotations of protein side chains, and intermolecular binding. However, this is exactly the time that the excited fluorescence state is maintained. Therefore, the fluorescence spectrum can be used to determine the number of binding sites, the binding constants, and the degree of synergy of protein-NPs binding (Hill constant) [29]. Additionally, it is sensitive to protein structure changes.

Proteins have three endogenous amino acid fluorophores for intrinsic fluorescence: tryptophan (Trp), tyrosine (Tyr), and phenylalanine (Phe) [30]. Because of their side-chain chromophores, they have different fluorescence excitation and emission spectra. Trp has the highest fluorescence intensity, Tyr the second, while Phe has the lowest. Under most experimental conditions, the quantum yield of Phe is very low, and its emission spectrum is rarely observed. Thus, the intrinsic protein fluorescence mainly depends on Trp and Tyr residues.

If the protein-NP complex does not have an endogenous fluorophore, a fluorescence probe must be added. A small fluorescent probe molecule is covalently or non-covalently bound to form a strongly fluorescent complex. Because the interaction between NPs and proteins usually changes the chemical environment of the fluorophore, or even its own structure, this changes the protein fluorescence and results in dynamic/static fluorescence quenching of the protein. Once the protein fluorescence is quenched, the fluorescence intensity diminishes, and the original emission peak shifts. The NP interactions with proteins can also be demonstrated by fluorescence-induced anisotropy [31] and fluorescence resonance energy transfer [32].

To quantify the fluorescence quenching Q, the following calculations are applied:

$$Q = (I_0 - I)/I_0, \tag{1}$$

where I_0 and I are fluorescence intensities in the absence and presence of Ag NPs, respectively. We assume the binding of proteins to NPs occurs at equilibrium, and we fit our data for Q to determine the equilibrium constant k_D for the protein-NPs interaction. Because a given protein can have multiple interactions with NPs,

a synergy effect in the binding equilibrium could occur. We consider this complex phenomenon by modeling Q from the Hill equations:

$$Q/Q_{max} = [NP]^n/(k_D^n + [NP]^n), \quad (2)$$

where Q_{max} is the saturation value of Q, k_D is the protein-NP equilibrium constant, and n is the Hill parameter. In a positive cooperative reaction ($n > 1$), once a protein is bound to the NP, its affinity for the NP increases in a super-linear trend. For a negative cooperative reaction ($n < 1$), the binding strength of the protein-NP complexes gradually weakens with the adsorption of other proteins. For non-cooperative associations, where $n = 1$ and Q formally have the mathematical form of the Langmuir adsorption equation, the affinity of the protein for the NP does not depend on whether other protein molecules are bound to it. The "binding constant" K is defined as the reciprocal of k_D. Because the protein-NP binding is at equilibrium, k_D is determined by fitting the fluorescence quenching data of Q to describe the interaction between Ag NPs and trypsin [33].

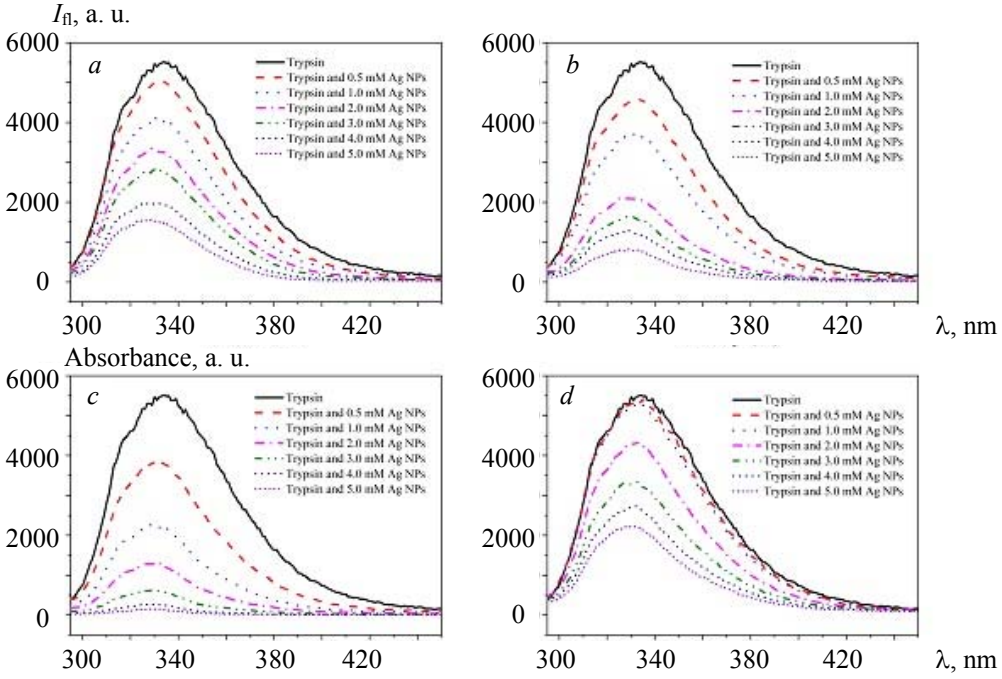

Fig. 3. Effect of different sizes (4 (a), 20 (b), 30 (c), and 45 nm (d)) of Ag NPs on the fluorescence spectra of trypsin ($T = 285$ K, pH 7.40, $\lambda_{ex} = 295$ nm); concentration (Ag NPs): 0, 0.5, 1.0, 2.0, 3.0, 4.0, and 5.0 mmol/L.

Figure 3 shows the fluorescence spectra of trypsin with fixed concentrations mixed with different concentrations of Ag NPs, and it shows the emission spectra of trypsin in the presence and absence of Ag NPs. As the diameters of the Ag NPs increased from 4 to 45 nm, they effectively quenched the trypsin fluorescence intensity. Additionally, the emission maximum intensity decreased with increased Ag NPs concentration. The fluorescence quenching effect indicates a transition to different electronic energy levels of the tyrosine, because the fluorescence wavelength depends on the energy difference between the energy levels. That is, the interaction of the chromophore with the surrounding group may change its excited-state energy, thereby changing the emission wavelength and intensity [34, 35]. The adsorption of trypsin on Ag NPs affects the binding between the chromophore (Trp or Tyr) in trypsin and the quencher (Ag NP). As the Ag NP concentration increases, the binding between Ag NPs and trypsin becomes stronger, which causes further protein conformation changes. As the Ag NPs surface binds with more amino acids, fluorescence quenching occurs more efficiently.

To observe the shifts in the maximum emission spectral band before the interaction, the fluorescence spectra of Ag NPs-trypsin complexes with Ag NPs sizes over the range 4–45 nm were normalized and sum-

marized in Fig. 4. Compared to that of the pure trypsin solution, the fluorescence spectra of the four different Ag NPs-trypsin complexes changed, indicating that the dielectric properties of the medium changed. A slight blue shift from 334 to 328 nm of the emission maximum wavelength was also observed, which may indicate that Ag NPs could quench the inner fluorescence of trypsin, and that the interaction between Ag NPs and trypsin indeed occurred.

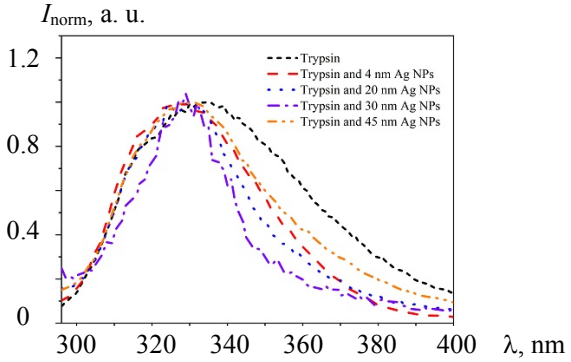

Fig. 4. Fluorescence quenching of trypsin by Ag NPs measuring normalized emission spectra of trypsin in the absence and presence of Ag NPs showing a shift of the emission peak.

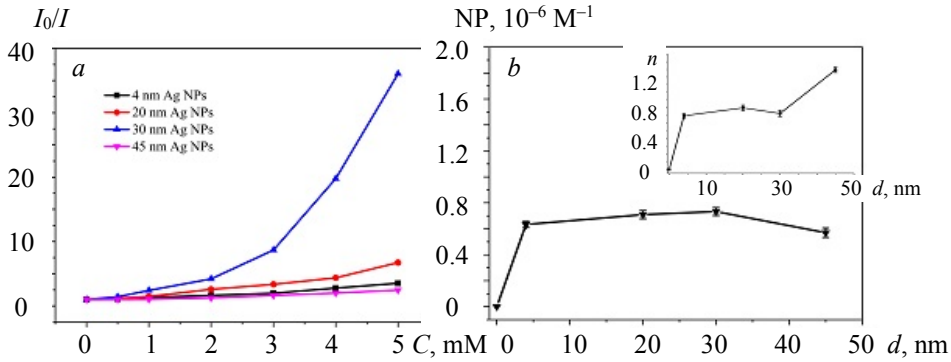

Fig. 5. Efficiency of fluorescence quenching of trypsin. a) Stern-Volmer plot of trypsin fluorescence quenching by Ag NPs having different sizes; b) effect of NP diameter. The inset shows the effect of NP size on the Hill coefficient, *n*, a quantitative measure of the cooperativity of mutual NP-protein binding.

In Figure 5a the relative kinetic efficiency of fluorescence quenching is estimated by fitting the dependence of I_0/I with the concentration of Ag NPs based on the Stern-Volmer formula:

$$I_0/I = 1 + k_{SV}[\text{NP}], \quad (3)$$

where k_{SV} is the quenching rate constant. After the binding between trypsin and the Ag NPs, the fluorescence quenching efficiency is lower for the smaller the Ag NP sizes at the same concentrations. This is because smaller Ag NPs with larger surface curvatures could decrease the amount of adsorbed protein. That is, the fluorescence quenching efficiency is proportional to the size of the Ag NPs, where more amino acids bind to the larger Ag NPs surfaces. However, the 45-nm Ag NPs exhibit lower fluorescence quenching efficiencies relative to the other three sizes (4, 20, and 30 nm), which may because the larger Ag NPs have lower relative surface area [36]. This reduces the number of absorbed proteins, resulting in reduced fluorescence quenching efficiency. As the concentration of Ag NPs increases, the Ag NPs with the same size have higher amounts of surface-bound protein and higher fluorescence quenching rates. Figure 6b quantitatively explores the binding properties of Ag NPs interacting with proteins. The binding constant is significantly dependent on protein properties and Ag NPs sizes, where the constants for trypsin increased progressively with Ag NPs diameter over the range 4–30 nm. A higher protein bulk density on the surfaces of the larger Ag NPs leads to a corresponding increase in binding constant *K*. Additionally, for the 45-nm Ag NPs, the binding association constants are lower than those smaller Ag NPs. This is because the volume interactions excluded within the ran-

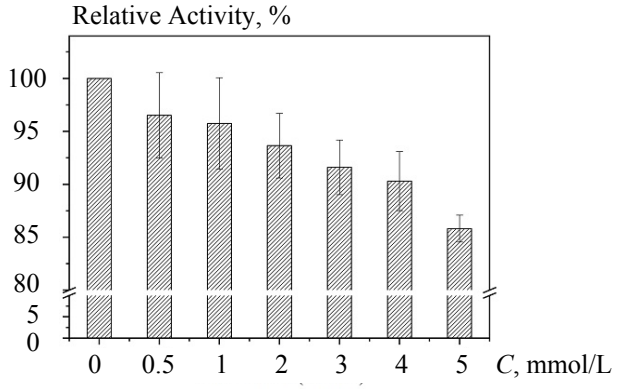

Fig. 6. Effect of Ag NPs on trypsin activity.

dom coiled nucleotide strands extending over the surface of the particle are enhanced, and the unfolded conformation of the protein should exhibit similar behavior. Therefore, less efficient protein adsorption was observed for the 45-nm Ag NPs. The Hill coefficient *n* was then applied to quantify the synergy effect for Ag NP and trypsin binding. The inset in Fig. 5b shows the Hill coefficient map of the complex and the relationship between the Hill coefficient *n* and the NP size. For trypsin and Ag NPs, $n < 1$ for the 4-, 20-, and 30-nm Ag NPs, while $n > 1$ for the 45-nm Ag NPs. This indicates that, for this absorption process, the binding energy of the proteins decreases on the surface of small NPs (4, 20, and 30 nm), while it increases on larger particles (45 nm) [37, 38].

The effects of mixing a range of concentrations of 30-nm Ag NPs with trypsin, measured before and after mixing for 5 min, 3 h, and overnight. The liquid was observed over four different time ranges. When the Ag NP solution was added to the trypsin solution, the silver sol became turbid instantaneously and maintained this state, which strongly indicated interaction between the Ag NPs and the trypsin and the formation of a protein corona. Furthermore, the interaction can affect the properties of both trypsin and Ag NPs.

Another important aspect of was the enzymatic activity of trypsin after the addition of Ag NP solution. After it was first mixed with the Ag NPs, the relative activity of trypsin was determined, as shown in Fig. 6. The enzymatic activity is slightly inhibited as the concentration of Ag NPs increased. Proteins have unique structures that determine their function and are stabilized by a variety of weak interactions, including hydrophobic, hydrogen bonding, and ionic [39]. Inhibitory activity suggests that Ag NPs may affect certain trypsin conformations. The slight inhibition may result from the Ag NPs properties such as high surface area or the high binding affinity to -HS bands in the protein. Furthermore, Ag NPs may also bind to the substrate [26], which could bring the trypsin and its substrate closer to increase the local enzyme concentration. Thus, there could be no significant inhibition of the enzyme activity.

Conclusions. The interactions between nanoparticles and protein molecules were characterized systematically with multiple methods to investigate the effects on protein structure functions, as well as on the biological effects of the nanoparticles. The effects of Ag NPs on trypsin molecules at different concentrations and sizes were characterized with CD, UV-Vis, and fluorescence spectroscopy. In the CD spectra, the trypsin secondary structure and conformation changed after interactions with Ag NPs. The α-helix increased slightly by 1.2%, the β-sheet decreased by 5.5%, the β-turn increased by 6.9%, and the random coil decreased slightly by 2.6%. In the UV-Vis spectra, the maximum absorption peaks of the Ag NPs shifted and the absorption intensity changed because the interaction between trypsin and Ag NPs may affect the particle size distributions and the surface plasma band of the NPs. Fluorescence spectra confirmed that the fluorescence quenching efficiency decreased with the NP size. As the Ag NP concentration increased, the same-size Ag NPs had higher surface binding ratios and higher fluorescence quenching rates of the protein. All the spectral results confirm that larger Ag NPs show an opposite tendency to that of smaller particles when affecting trypsin fluorescence. In macroscopic behavior detection, the solution exhibits color change as the Ag NP concentration increased, and agglomeration occurred. Form these results, it was confirmed that Ag NPs interact effectively with trypsin and form protein coronas. Both the concentration and size changes of the Ag NPs can affect the trypsin structure and thus induce spectral changes. In combination with specific applications, the biosafety of NPs should be considered with their other properties to reduce toxicity. This study has provided an understanding of the interaction mechanism of Ag NPs with trypsin, and could provide theoretical support for NP applications in the fabrication of biosafety nanomaterials to reduce its biological toxicity.

Acknowledgements. The authors wish to thank the Natural Science Foundation of Jiangsu Province (BK20191294), the National Natural Science Foundation of China (21505074), and the Fundamental Research Funds for the Central Universities (30919011214) for partial support of this work.

REFERENCES

1. G. Mustafa, S. Komatsu, *Curr. Proteomics*, **14**, No. 1, 3–12 (2017).
2. Y. W. Wang, J. S. Kim, G. H. Kim, K. S. Kim, *Appl. Phys. Lett.*, **88**, 143106 (2006).
3. J. Varalda, C. A. Dartora, A. J. A. de Oliveira, W. A. Ortiz, B. Vodungbo, M. Marangolo, F. Vidal, Y. Zheng, G. G. Cabrera, D. H. Mosca, *Phys. Rev. B*, **83**, 045205 (2011).
4. Y. Z. Liu, Y. T. Hu, R. S. Chen, W. T. Zhan, H. W. Ni, P. M. Zhang, F. Liang, *Curr. Nanosci.*, **12**(999), 1–10 (2015).
5. D. Zhang, O. Neumann, H. Wang, V. M. Yuwono, A. Barhoumi, M. Perham, J. D. Hartgerink, P. Wittung-Stafshede, N. J. Halas, *Nano Lett.*, **9**, 666–671 (2009).
6. I. Lynch, K. A. Dawson, *Nano Today*, **3**, No. 1-2, 40 (2008).
7. C. Nilofer, A. Sukhwal, A. Mohanapriya, P. Kangueane, *Bioinformation*, **13**, No. 6, 164–173 (2017).
8. W. He, H. J. Dou, L. Zhang, L. J. Wang, R. Y. Wang, J. B. Chang, *Spectrochim. Acta A*, **173**, 188–195 (2017).
9. S. T. Yang, Y. Liu, Y. W. Wang, A. N. Cao, *Small*, **9**, No. 9-10, 1635–1653 (2013).
10. X. R. Li, Y. H. Yan, X. D. Cheng, W. Guo, Y. R. Peng, *Int. J. Biol. Macromol.*, **114**, 836–843 (2018).
11. R. Concalves, N. Mateus, I. Pianet, M. Laguerre, V. D. Freitas, *Langmuir*, **27**, 13122–13129 (2011).
12. L. Gombos, J. Kardos, A. Patthy, P. Medveczky, L. Szilágyi, A. Málnási-Csizmadia, L. Gráf, *Biochemistry*, **47**, No. 6, 1675–1684 (2008).
13. Y. Wan, Z. R. Guo, X. L. Jiang, K. Fang, X. Lu, Y. Zhang, N. Gu, *J. Colloid Interface Sci.*, **394**, 263–268 (2013).
14. W. R. Wang, R. R. Zhu, R. Xiao, H. Liu, S. L. Wang, *Biol. Trace Elem. Res.*, **142**, No. 3, 435–446 (2011).
15. P. D. Pino, B. Pelaz, Q. Zhang, P. Maffre, G. U. Nienhaus, W. J. Parak, *Mater. Horiz.*, **1**, 301 (2014).
16. S. S. Li, B. Q. Li, J. J. Liu, S. H. Lu, H. L. Zhai, *Proteins*, **86**, 751–758 (2018).
17. S. Gautam, P. Dubey, M. N. Gupta, *Colloids Surf. B*, **102C**, 879–883 (2012).
18. A. Gebregeorgis, C. Bhan, O. Wilson, D. Raghavan, *J. Colloid Interface Sci.*, **389**, No. 1, 31–41 (2013).
19. S. Navea, R. Tauler, E. Goormaghtigh, A. D. Juan, *Proteins: Struct., Funct., Bioinform.*, **63**, 527–541 (2006).
20. N. J. Greenfield, *Nat. Protoc.*, **1**, No. 6, 2876–2890 (2007).
21. L. Whitmore, B. A. Wallace, *Biopolymers*, **89**, No. 5, 392–400 (2008).
22. L. N. Geng, X. Wang, N. Li, M. H. Xiang, K. Li, *Colloids Surf. B*, **34**, No. 4, 231–238 (2004).
23. V. M. Bolanos-Garcia, S. Ramos, R. Castillo, J. Xicohtencatl-Cortes, J. Mas-Oliva, *J. Phys. Chem. B*, **105**, 5757 (2001).
24. J. Huang, Y. Z. Yuan, H. Liang, *Sci. China, Ser. B*, **46**, 387 (2003).
25. P. M. Tessier, J. Jinkoji, Y. C. Cheng, J. L. Prentice, A. M. Lenhoff, *J. Am. Chem. Soc.*, **130**, 3106–3112 (2008).
26. M. Lv, E. G. Zhu, Y. Y. Su, Q. N. Li, W. X. Li, Y. Zhao, Q. Huang, *Prep. Biochem. Biotechnol.*, **39**, 429–438 (2009).
27. C. Wang, Q. H. Wu, C. R. Li, Z. Wang, *Anal. Sci.*, **23**, No. 4, 429–433 (2007).
28. Q. X. Mu, W. Liu, Y. H. Xing, H. Y. Zhou, Z. W. Li, Y. Zhang, L. H. Ji, F. Wang, Z. K. Si, B. Zhang, B. Yan, *J. Phys. Chem. C*, **112**, 3300–3307 (2008).
29. X. Y. Xie, Z. W. Wang, X. M. Zhou, X. R. Wang, *J. Hazard. Mater.*, **192**, No. 3, 1291–1298 (2011).
30. K. Sirine, A. J. Merrell, B. D. Ray, H. I. Petrach, *Biophys. J.*, **106**, No. 2, 513a (2014).
31. L. Song, H. N. Wang, S. W. Wang, H. Zhang, H. L. Cong, P. Tien, *J. Mater. Sci.*, **49**, No. 7 (2014).
32. H. Li, M. Wang, C. Z. Wang, W. Li, W. B. Qiang, H. Li, *Anal. Chem.*, **85**, No. 9 (2013).
33. S. H. D. Paoli, J. J. Park, C. W. Meuse, D. Pristinski, M. L. Becker, A. Karim, J. F. Douglas, *ACS Nano*, **4**, No. 1, 365–379 (2009).
34. T. B. Yuan, A. Weljie, H. J. Vogel, *Biochemistry*, **37**, No. 9, 3187–3195 (1998).
35. Y. Q. Wang, H. M. Zhang, G. C. Zhang, Q. H. Zhou, *J. Mol. Struct.*, **886**, No. 1-3, 77–84 (2008).
36. W. Norde, *Colloids Surf. B*, **61**, No. 1, 1–9 (2008).
37. P. K. Jain, W. Y. Huang, M. A. EI-Sayed, *Nano Lett.*, **7**, No. 7, 2080–2088 (2007).
38. Y. Ikeda, N. Taniguchi, T. Noguchi, *J. Biol. Chem.*, **275**, No. 13, 9150–9156 (2000).
39. K. A. Dill, *Biochemistry*, **29**, No. 31, 7133–7155 (1990).

Supporting information

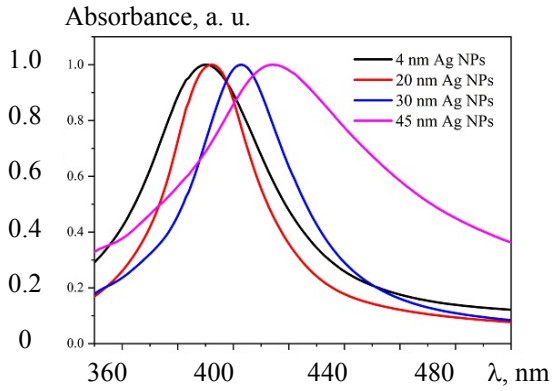

Fig. S1. Normalized UV-Vis spectra of different sizes of Ag NPs; the maximum absorption peak is at 390, 392, 403, and 414 nm, respectively.

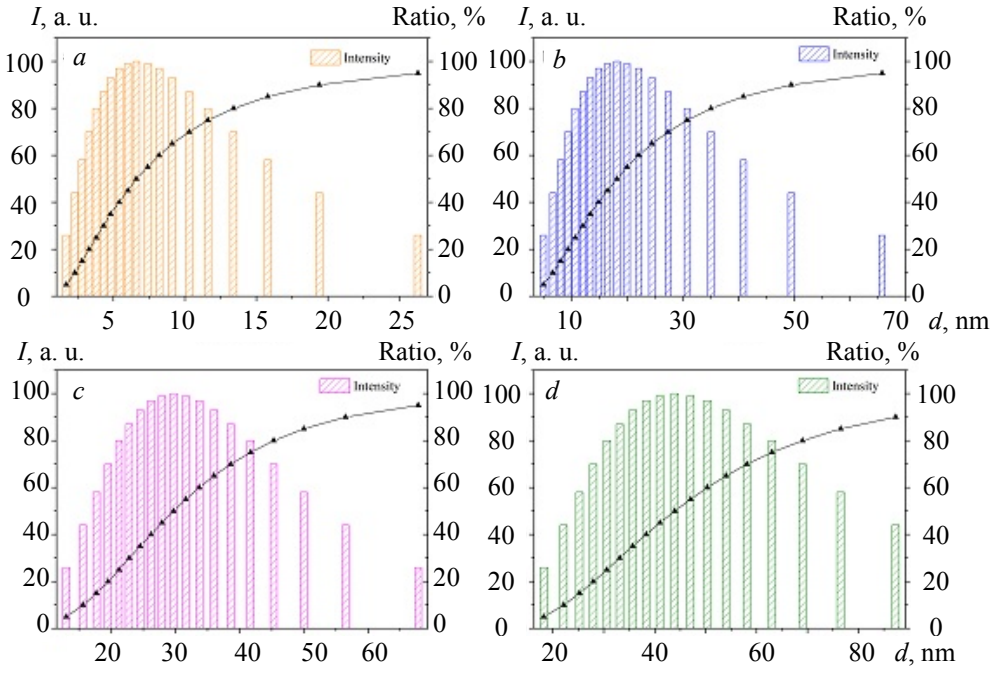

Fig. S2. Distributions of the relative intensity and relative ratio of Ag NPs with respect to their diameter *d* of 4 (a), 20 (b), 30 (c), and 45 nm (d).

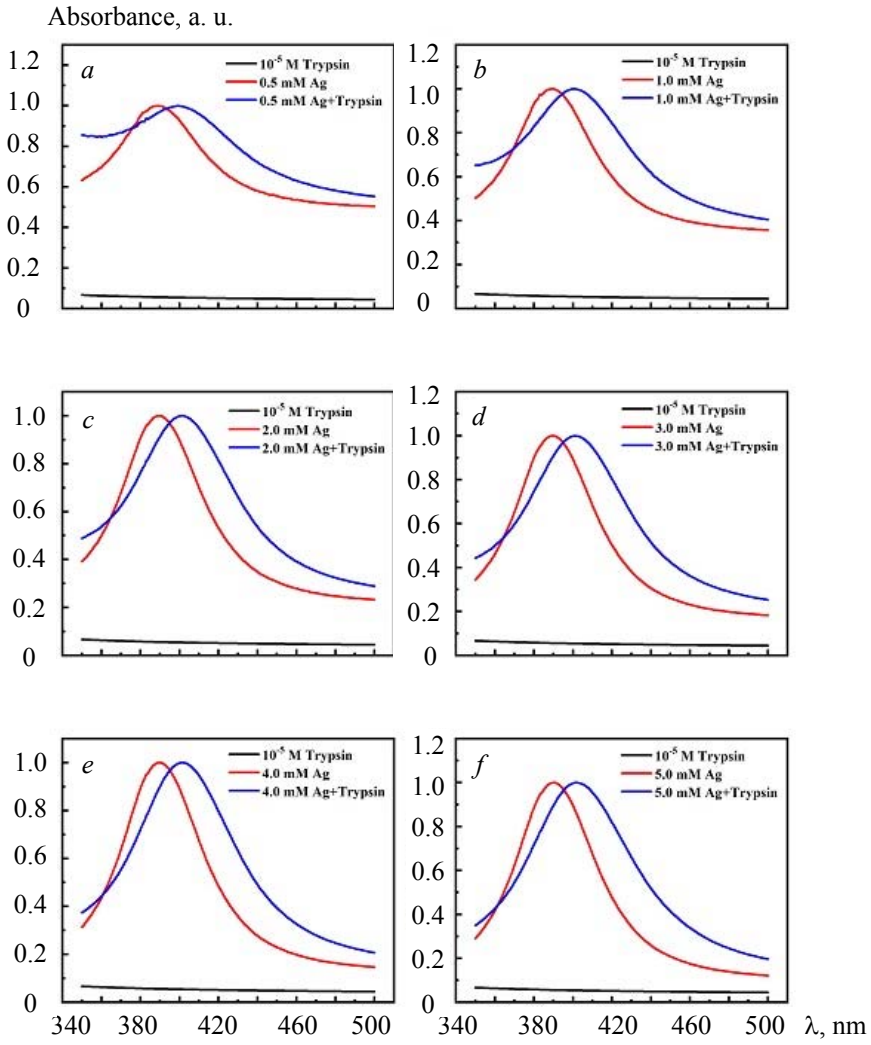

Fig. S3. Normalized UV-Vis spectra of 4 nm Ag NPs concentration from 0.5–5.0 mmol/L in the absence and presence of trypsin, respectively. The trypsin concentration is 1.0×10^{-5} mol/L.

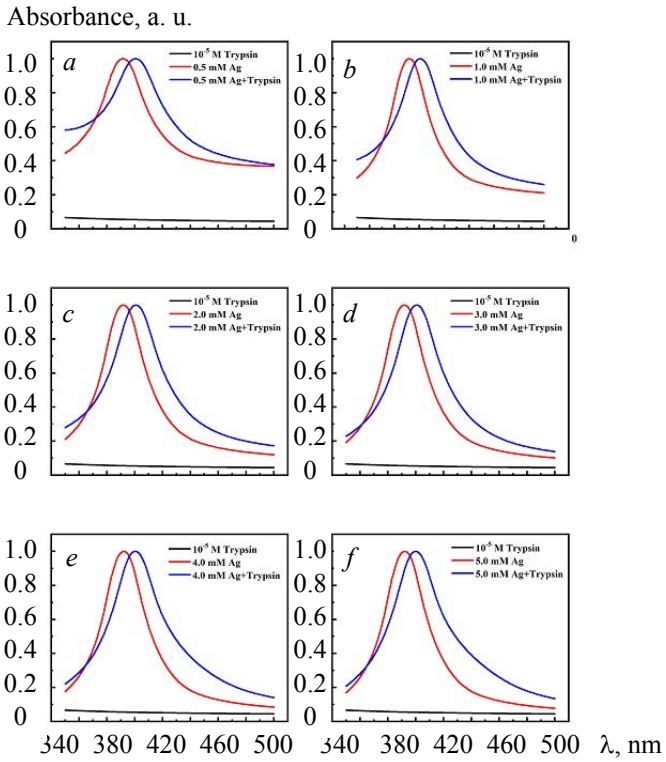

Fig. S4. Normalized UV-Vis spectra of 20 nm Ag NPs concentration from 0.5–5.0 mmol/L in the absence and presence of trypsin, respectively. The trypsin concentration is 1.0×10^{-5} mol/L.

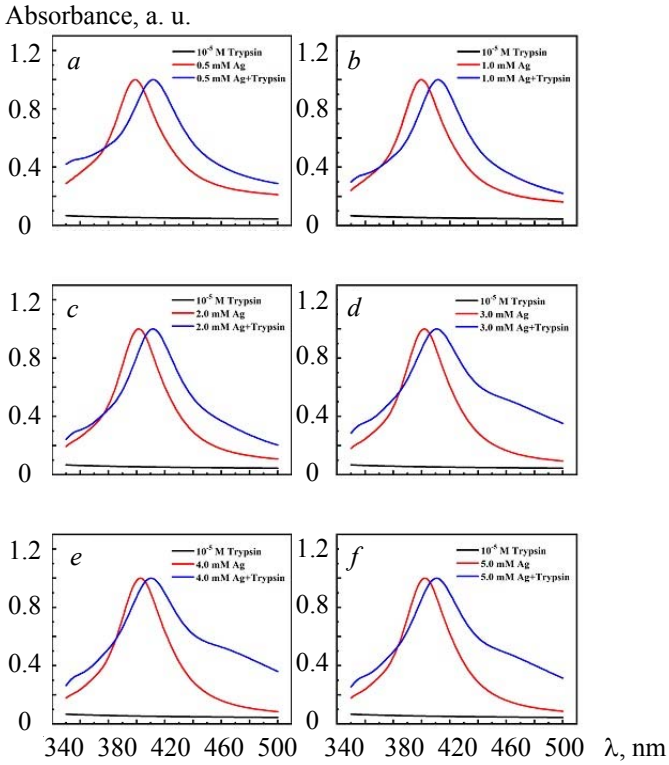

Fig. S5. Normalized UV-Vis spectra of 30 nm Ag NPs concentration from 0.5–5.0 mmol/L in the absence and presence of trypsin, respectively. The trypsin concentration is 1.0×10^{-5} mol/L.

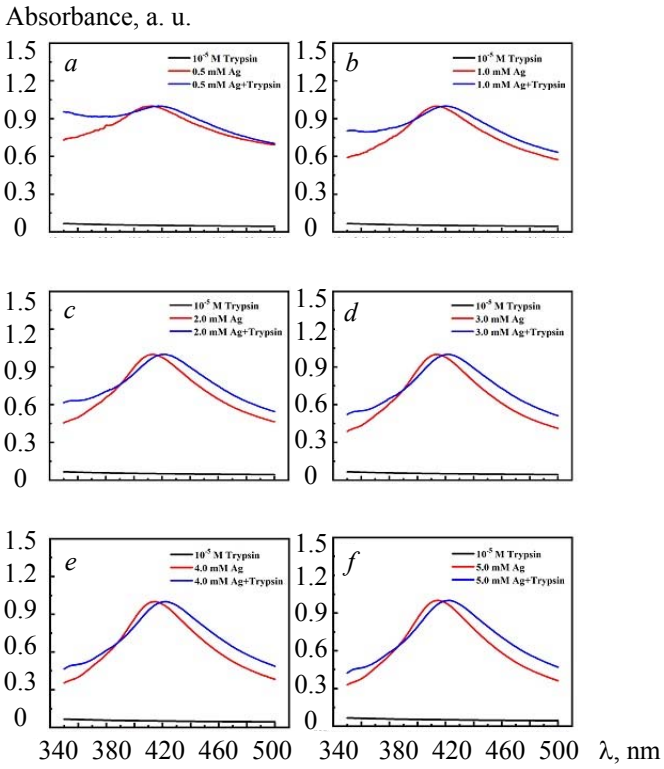

Fig. S6. Normalized UV-Vis spectra of 45 nm Ag NPs concentration from 0.5–5.0 mmol/L in the absence and presence of trypsin, respectively. The trypsin concentration is 1.0×10^{-5} mol/L.